Validation of Sea Ice Motion from QuikSCAT with those from SSM/I and Buoy

Yunhe Zhao, Antony K. Liu, and David G. Long, *Senior Member, IEEE*

***Abstract*—Arctic sea ice motion for the period from October 1999 to March 2000 derived from QuikSCAT and special sensor microwave/imager (SSM/I) data using the wavelet analysis method agrees well with ocean buoy observations. Results from QuikSCAT and SSM/I are compatible when compared with buoy observations and complement each other. Sea ice drift merged from daily results from QuikSCAT, SSM/I, and buoy data gives more complete coverage of sea ice motion. Based on observations of six months of sea ice motion maps, the sea ice motion maps in the Arctic derived from QuikSCAT data appear to have smoother (less noisy) patterns than those from NSCAT, especially in boundary areas, possibly due to constant radar scanning incidence angle. For late summer, QuikSCAT data can provide good sea ice motion information in the Arctic as early as the beginning of September. For early summer, QuikSCAT can provide at least partial sea ice motion information until mid-June. In the Antarctic, a case study shows that sea ice motion derived from QuikSCAT data is consistent with pressure field contours.**

***Index Terms*—QuikSCAT, sea ice motion, special sensor microwave/imager (SSM/I), wavelet transform.**

I. Introduction

QUIKSCAT, a "quick recovery" mission to fill the gap created by the loss of data from the NASA Scatterometer (NSCAT), when the ADEOS-1 satellite lost power in June 1997, was launched on June 19, 1999. QuikSCAT is an active sensor, and the sensor footprint is an ellipse 25 km $\times$ 37 km. In both the Arctic and the Antarctic regions, repeated footprints of the satellite make it possible to construct QuikSCAT images with a 12.5 km grid and finer resolution (e.g., see [1]). In this paper, the daily (estimated over a four-day sliding window for the Arctic and over a one-day sliding window for the Antarctic) sea ice motion derived from QuikSCAT using an ice-tracking algorithm based on wavelet transform is demonstrated, and the applications of the daily sea ice motion are indicated. The uncertainty of QuikSCAT-derived sea ice motion is determined from validation with those from *in situ* buoy data and Defense Meteorological Satellite Program (DMSP) special sensor microwave/imager (SSM/I) observations during the same period of time. The instrument differences between QuikSCAT and NSCAT lead to significantly different spatial and temporal sampling characteristics, and it is for this reason that QuikSCAT ice motion validation is required. NSCAT is a fan-beam scatterometer with fixed azimuth but variable incidence, while QuikSCAT has fixed incidence and variable azimuth.

Satellite observations provide more complete and routine coverage of polar region than observations from any other means, and they have been used by several authors in deriving polar sea ice drift (e.g., see [2] and references cited there). The efficiency and utility of wavelet transform in analyzing nonlinear dynamical ocean systems has also been documented in several papers ([2] and references cited there). In Section II, wavelet analysis for ice feature tracking and sea ice motion from QuikSCAT and SSM/I data are presented. Wavelet analysis results from QuikSCAT and SSM/I are compared with the ice motion derived from buoys for validation in Section III. Section IV deals with the potential application of QuikSCAT data in summer ice tracking. Section V is devoted to a sea-ice-tracking case study for the Antarctic using QuikSCAT data. The results and applications of satellite-derived sea ice motion are discussed and summarized with previous NSCAT and SSM/I data in the final section.

II. Wavelet Analysis of Satellite Images

A sea-ice-tracking procedure based on wavelet transform of satellite data and its error analysis have appeared in [2]–[4]. The effect of wavelet transform is a bandpass filter with a threshold for feature detection. For the details of the procedure, we refer readers to [2]–[4]. In this study, the same procedure is applied to QuikSCAT and SSM/I data with a few modifications. For the Arctic, QuikSCAT images with 12.5 km pixel size are first constructed from QuikSCAT Level 2A data, and SSM/I images are obtained from SSM/I compact discs. QuikSCAT Sigma-0 data has an incidence angle either around 54.24° (v-polarization) or around 46.44° (h-polarization) within $\pm 0.5°$. Only v-polarization Sigma-0 data with an incidence angle around 54.24° are used in the construction of QuikSCAT images because of its better coverage. Areas indicated by sea ice flags in QuikSCAT data as land, open ocean, or no-data areas are masked in the images. For the Antarctic case study, the QuikSCAT data are processed with a scatterometer image reconstruction (SIR) resolution enhancement algorithm to a pixel resolution of 4.45 km from QuikSCAT Level 1B data [1], and sea ice extent is determined using the method of [5]. The QuikSCAT design specifications for location accuracy requirements are 25 km (rms)

Manuscript received April 12, 2001; revised April 3, 2002. This work was an Ocean Vector Wind Science Team (OVWST) Project and was supported by the National Aeronautics and Space Administration.

Y. Zhao is with Caelum Research Corporation and also with the Oceans and Ice Branch, NASA Goddard Space Flight Center, Greenbelt, MD 20771 USA (e-mail: yunhe@neptune.gsfc.nasa.gov).

A. K. Liu is with the Oceans and Ice Branch, NASA Goddard Space Flight Center, Greenbelt, MD 20771 USA (e-mail: liu@neptune.gsfc.nasa.gov).

D. G. Long is with the Electrical and Computer Engineering Department, Brigham Young University, Provo, UT 84602 USA (e-mail: long@ee.byu.edu).

Publisher Item Identifier 10.1109/TGRS.2002.800442.

absolute and 10 km (rms) relative. However, the actual performance is currently estimated to be better than 6 km (rms) absolute and less than 1 km (rms) relative with bias dominating the total error [6]. Thus, QuikSCAT has very high precision measurement locations, far exceeding its design specifications and enabling the application of resolution enhancement algorithms. For both cases, wavelet transform is then applied to the satellite image at various scales to separate various ice textures or features. In the Arctic, two tracking regions are considered: coast/bay for fast ice motion (with a two-day sliding window), and central Arctic for slow ice motion (with a four-day sliding window). Template matching is performed with the results from the wavelet transform of the images between day 1 and day 5 for the central Arctic and between day 2 and day 4 for the coast/bay. In the Antarctic, template matching is performed with the results from the wavelet transform of the images between day 1 and day 2. For both cases, velocities are estimated by dividing the displacement over the time interval. Finally, the sea ice drift map can be merged by block average with outlier filtering. The outlier filtering after block average is performed as follows: at any location, the mean velocity of nine neighboring ice velocities is computed. If the angle between the mean ice velocity and the ice velocity at the location is bigger than a certain degree, then the ice velocity at the location is discarded.

Fig. 1(a) and (b) show sea ice drift maps of the Arctic Ocean for November 5, 1999, derived from SSM/I and QuikSCAT data, respectively, where thin white arrows indicate velocities derived from satellite data, while thick white arrows indicate velocities derived from buoy data. Two circulation patterns—one in the Beaufort Sea and the other across the Chukchi, Beaufort, and Laptev Seas—are clearly observed in the maps. The ice motion converges in an area between the Chukchi Sea and the Beaufort Sea. Notice that velocities derived from both QuikSCAT and SSM/I data agree well with those from buoy data. Wavelet transform scales used in deriving these images from QuikSCAT and SSM/I data are based on parameter study and testing and are 1.0, 2.42, and 2.828. The resultant ice velocities have been block averaged to a 100 km $\times$ 100 km grid with outlier filtering. The empty areas with no velocity in the map indicate the regions where the tracking procedure cannot be used, since no matching templates between the time periods can be determined. Clearly, the ice motion maps derived from QuikSCAT and SSM/I data for November 5, 1999 are complementary to each other. The regions without ice velocity data from QuikSCAT and SSM/I are generally not colocated, since the QuikSCAT and SSM/I data correspond to different physical features: surface roughness and brightness–temperature anomalies, respectively. For the period from October 1999 to March 2000, based on the observations of sea ice motion maps, the patterns of motion from QuikSCAT appear smoother than those from SSM/I.

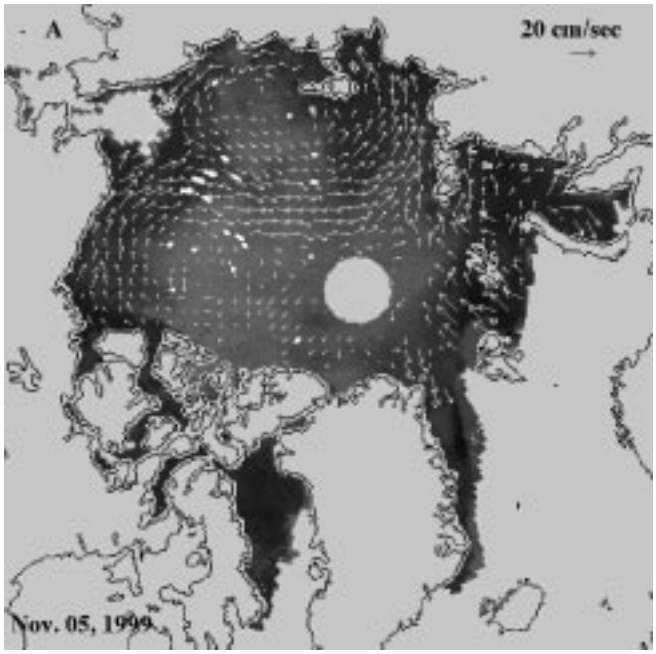

(a)

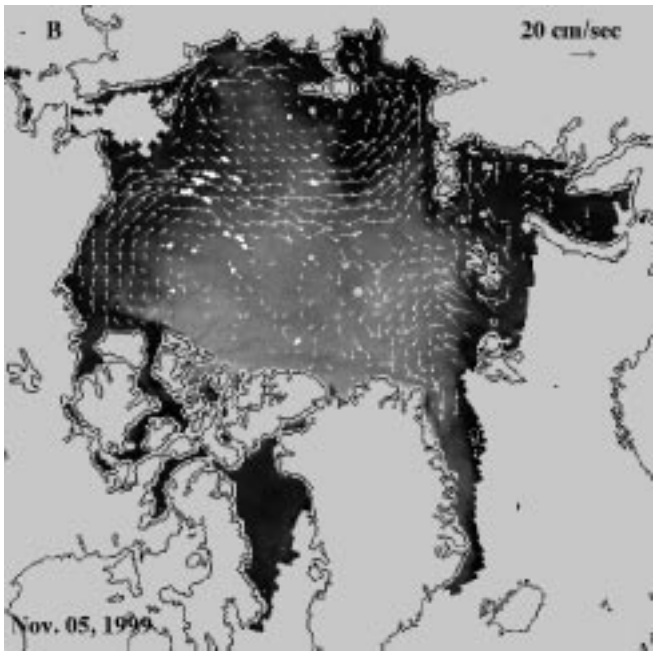

(b)

Fig. 1. Arctic sea ice drift maps of the Arctic basin in a grid of 100 $\times$ 100 km derived from (a) SSM/I 85 GHz radiance data and (b) from QuikSCAT data on November 5, 1999. Thin white arrows indicate velocities derived from feature tracking using wavelet analysis, while thick white arrows indicate velocities from buoys.

III. Data Comparisons

Liu *et al.* [2] has made a detailed quantitative comparison between the ice drift derived from NSCAT and SSM/I, with those from buoy data for November and December, 1996. They found that ice drift derived from NSCAT or SSM/I agreed well quantitatively with those from buoy data. Following their approach, in this paper we compared QuikSCAT- and SSM/I-derived ice velocities with buoy data in the same period. Section VI discusses and summarizes a six-month data comparison between QuikSCAT, NSCAT, and SSM/I with buoy-derived ice drift.

To quantitatively compare the ice drift derived from QuikSCAT and SSM/I data with buoy data, for each ice velocity derived from buoy data, the closest (within 50 km) satellite-derived ice velocity is identified. Since the pixel sizes of both QuikSCAT and SSM/I images for the Arctic are

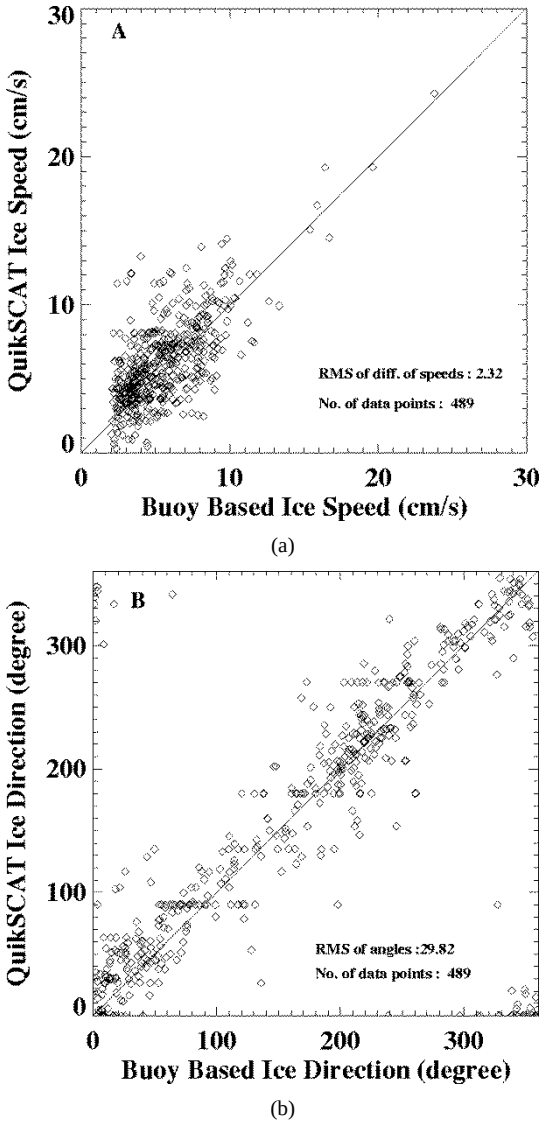

Fig. 2. QuikSCAT versus buoy (a) ice speed and (b) ice drift direction in November and December, 1999. The dashed line indicates a perfect fit.

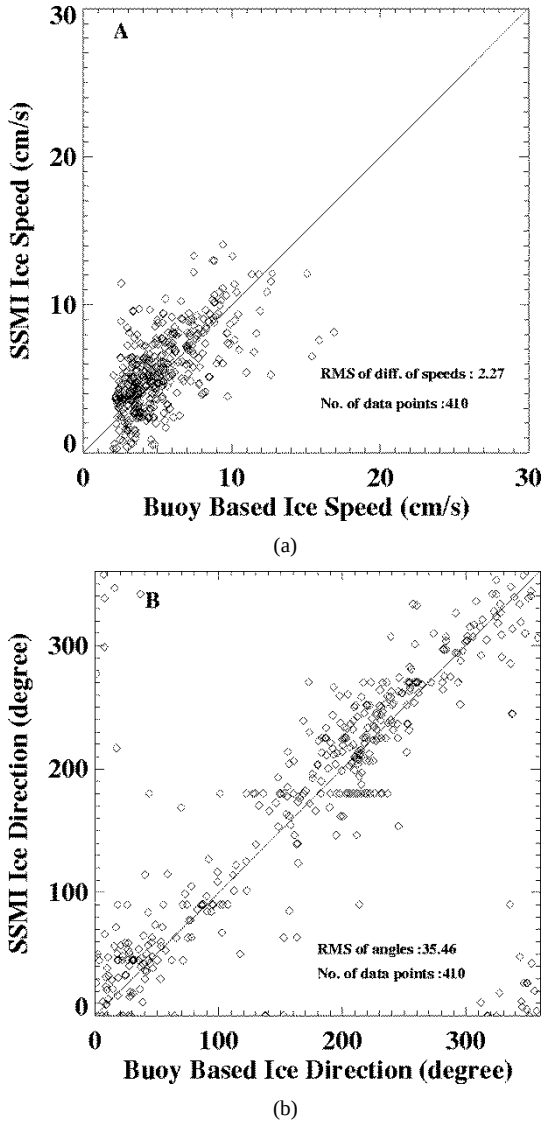

Fig. 3. SSM/I versus buoy (a) ice speed and (b) ice drift direction in November and December, 1999. The dashed line indicates a perfect fit.

12.5 km, and since a four-day sliding window is used in the ice-tracking procedure, the minimum discernable displacement is 6.25 km in four days, or 1.8 cm/s, and the maximum displacement error due to the resolution is 6.25×1.414 km in four days, or 2.5 cm/s. The uncertainty of sea ice tracking from satellite data also includes other factors, such as the displacement noise due to the grid cell size quantization (see [2], [8], [9] for more detail). Moreover, ice velocities derived from satellite data have larger direction errors for slowly moving sea ice features because location errors of end-points have more significant effects for shorter displacement vectors [2]. Therefore, buoy-derived ice velocities with speed less than 2 cm/s are not included in the comparison. The root mean square of the speed and direction differences between all buoy-derived velocities with speed greater than 2 cm/s and their corresponding QuikSCAT- or SSM/I-derived velocities are computed for November and December, 1999.

The root means square of the speed difference between buoy-derived ice velocities with speed greater than 2 cm/s and their corresponding QuikSCAT-derived ice velocities for November and December, 1999, is 2.32 cm/s with 489 data points, as shown in Fig. 2. The proximity of the linear fit to the dashed line (the ideal fit) shows that there is an extremely good match for speed. The rms direction difference is 29.82°. This comparison result is consistent with the one between buoy-derived and NSCAT-derived ice velocities for November and December, 1996 in [2]. Fig. 3 shows that the rms of the speed difference and the rms of the direction differences between buoy-derived ice velocities and SSM/I-derived ones for November and December, 1999 are 2.27 cm/s and 35.46°, respectively, with 410 data points. This comparison result is also consistent with the one between buoy-derived and SSM/I-derived ice drift for November and Decembe, 1996 in [2]. Note that the comparison results between QuikSCAT and buoy and between SSM/I and buoy are comparable, although the rms of the direction differences between SSM/I-derived and buoy-derived ice velocities is slightly larger than between QuikSCAT and buoy.

Since the ice velocities derived from QuikSCAT and SSM/I are comparable and complement each other, the three ice drift

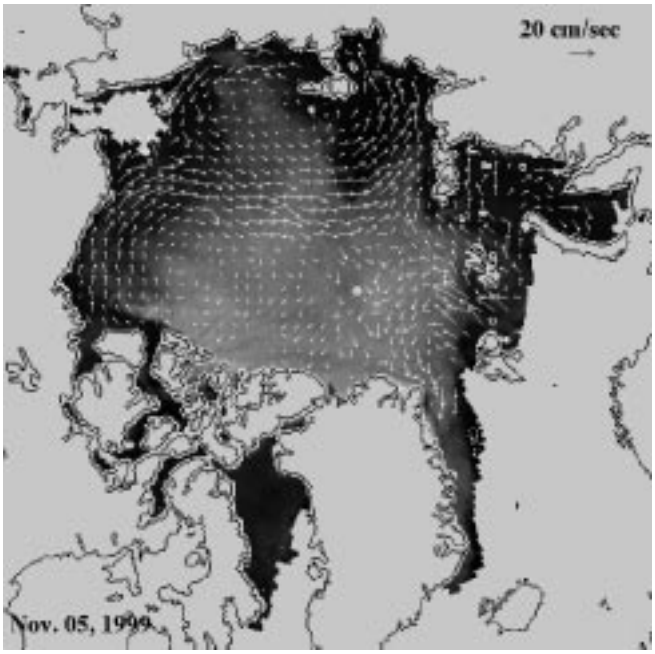

Fig. 4. Merged Arctic sea ice motion map on November 5, 1999.

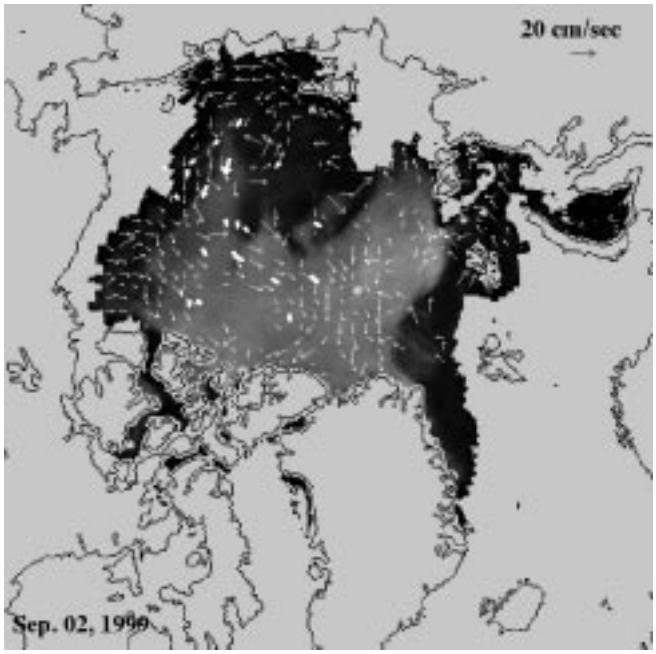

Fig. 5. Arctic sea ice drift map of the Arctic basin in a grid of 100×100 km derived from QuikSCAT data on September 2, 1999. Thin white arrows indicate velocities derived from feature tracking using wavelet analysis, while thick white arrows indicate velocities from buoys.

results from QuikSCAT, SSM/I, and buoy can be merged to generate composite maps with more complete coverage of sea ice motion. Fig. 4 shows a merged sea ice motion map for November 5, 1999. Clearly, the merged sea ice motion map has more complete coverage of sea ice motion than Fig. 1(a) and (b). In merging sea ice velocities derived from QuikSCAT, buoy, and SSM/I, buoy-derived ice velocities are merged with their closest satellite-derived ice velocities (they are usually not in the same locations), and a weighted-average has been applied with weights of $1/3, 1/2$, and $1/6$ assigned to QuikSCAT, buoy, and SSM/I, respectively. The assigned weights are based on the estimated uncertainties for each instrument (e.g., rms values). The time series of the merged daily sea ice drift maps for the period from October 1999 to March 2000 (not shown) indicates that the ice motion field changes significantly for every four to seven days.

IV. Summer Ice Tracking in the Arctic

During the Arctic summer, because of melting and ponding, two sequential daily satellite images may appear very different in their numbers of features and their sizes and shapes. Therefore, feature tracking based on finding common features in two sequential images is difficult during the summer months. However, in early summer, before melting becomes very rapid and in late summer when sea ice melting slows down and a new sea ice is beginning to form, QuikSCAT is capable of providing sea ice motion information using the wavelet-transform-based ice-tracking procedure. Fig. 5 shows the sea ice motion map derived from QuikSCAT data for September 2, 1999. The sea ice motion pattern from QuikSCAT agrees quite well with sea ice drift derived from buoy data, although there are some empty areas in the map. For September, 1999, the rms of the speed differences between QuikSCAT-derived and buoy-derived ice velocities is 3.80 cm/s with 245 data points, and the rms of the direction differences between them is 46.31°. However, SSM/I data are not able to provide as much sea ice motion information as QuikSCAT in September, 1999. For the early summer of 2000, QuikSCAT is able to track sea ice motion at least partly (about 50%) in the Arctic until June 15, 2000.

V. Antarctic Case

Wavelet-transform-based ice tracking has been used to derive sea ice motion in the Antarctic using SSM/I data [3]. As a case study, this procedure is applied to QuikSCAT data to derive sea ice motion in the Antarctic on October 4, 1999. In the Antarctic, sea ice tracking is much more difficult than in the Arctic because most of the sea ice cover is formed of smooth first-year ice with only a few small-scale and short-lived features to track. Since around the Antarctic continent the sea ice is free to drift without a land boundary, the sea ice variability and motion in the Antarctic are generally much larger than in the Arctic basin. Therefore, to track the ice texture and resolve the ice drift velocity, QuikSCAT egg images of the Antarctic with a resolution of 4.45 km through enhanced processing by the Scatterometer Climate Record Pathfinder (SCP) project at Brigham Young University, UT, [7] together with a one-day sliding window, are used to obtain better results. Since there is insufficient data to perform a comprehensive validation in the Antarctic, sea ice velocities derived from QuikSCAT data in the Antarctic on October 4, 1999 are compared with mean sea level pressure field contours derived from National Oceanic Atmospheric Administration (NOAA) National Center for Environmental Prediction–National Center for Atmospheric Research (NCEP–NCAR) Climate Data Assimilation System 1 (CDAS-1) daily intrinsic mean sea level pressure data of the same day as shown in Fig. 6, where white arrows are the sea

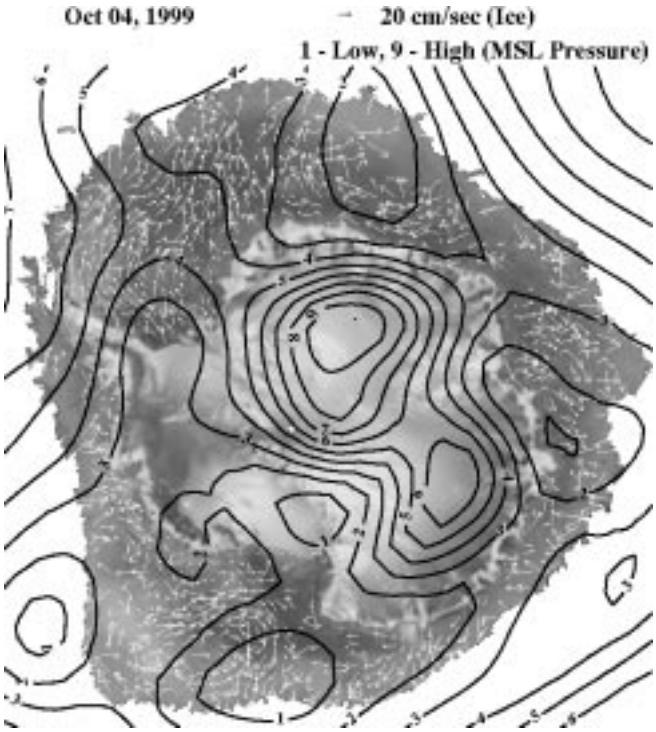

Fig. 6. Composite map of mean sea level pressure field contours and sea ice velocities derived from QuikSCAT data in the Antarctic on October 4, 1999.

TABLE I
COMPARISON OF SATELLITE-DERIVED AND BUOY-DERIVED SEA ICE MOTION

	NSCAT (10/96-03/97)	QuikSCAT (10/99-03/00)	SSMI (10/92-03/93)	SSMI (10/96-03/97)	SSMI (10/99-03/00)
RMS (speed difference)	2.86 cm/s	2.85 cm/s	2.54 cm/s	2.97 cm/s	2.83 cm/s
RMS (direction difference)	25.51º	28.25º	27.09º	30.63º	33.17º
Points	1029	1360	2196	1059	1040

All buoy-derived sea ice velocities with speed less than or equal to 2 cm/s are excluded. For the period 10/92-03/93, if all ice velocities are used in the comparison, then the rms of speed differences between SSM/I-derived and buoy-derived velocities is 2.52 cm/s with 2490 data points, and the rms of direction differences is 34.89º [9].

ice velocities and pressure field contours are drawn in black. Note that the sea ice motions derived from QuikSCAT data, in general, are well correlated with pressure field contours. Therefore, in the Antarctic, the wavelet-transform-based ice-tracking procedure is capable of sea ice tracking.

VI. DISCUSSION

To further examine satellite-data-derived sea ice motion, Table I summarizes some six-month comparison results of sea ice motion derived from SSM/I, NSCAT, and QuikSCAT with those derived from buoy data for different periods. For all comparison periods, the rms of the speed differences between buoy-derived ice velocities and satellite-derived ones are all under 3 cm/s, and the rms of the direction differences between them are around 30°. Moreover, all satellite-derived sea ice motion data sets are consistent and comparable.

It is clear that sea ice motion products derived from SSM/I, NSCAT, and QuikSCAT data have very good quantitative agreements with the ice motion products derived from buoy data. But, the sea ice motion products derived from NSCAT and QuikSCAT data are slightly more accurate than that derived from SSM/I data because both NSCAT and QuikSCAT are active sensors and do not suffer from cloud and atmospheric effects. Also, the results from NSCAT and QuikSCAT are very consistent. The rms of the direction difference between NSCAT-derived and buoy-derived ice drift for the period from October, 1996 to March, 1997 is slightly better than that between QuikSCAT-derived ice velocities and buoy-derived ones for the same winter period in 1999 and 2000. But keep in mind that the rms are for two different periods and that the ice motion in the central Arctic during winter 1999 has a very slow motion, and so the ice-tracking results are less accurate. In fact, based on the observations, the ice motion maps from QuikSCAT data appear to have smoother patterns than those from NSCAT, especially in boundary areas, e.g., in the Kara and Barents Seas where there is no buoy for comparison. The smoother patterns may be due to the fact that QuikSCAT data have constant scanning incidence angles, eliminating a potential error associated with incidence angle correction associated with the construction of satellite images and thus minimizing noise and tracking error. The comparison suggests that merged sea ice motions from QuikSCAT, SSM/I, and buoy data are suitable for the computation of deformation. A method for computing and comparing divergence and shear at the large scale between buoys and SSM/I has been developed by [10], and the minimum rms difference for deformation are found to scale with the temporal and spatial uncertainties of the SSM/I, suggesting that even better results can be achieved with higher-resolution instruments such as AMSR (advanced microwave scanning radiometer).

ACKNOWLEDGMENT

The authors wish to thank Tim Liu of Jet Propulsion Laboratory/CIT for his encouragement and for providing the QuikSCAT data via the PO.DAAC. QuikSCAT images with resolution 4.45 km from enhanced processing are available for public use at the SCP project's Web site www.scp.byu.edu at Brigham Young University, UT. The DMSP SSM/I data were acquired on CD-ROM from the National Snow and Ice Data Center in Boulder, CO. The Arctic Ocean Buoy data were downloaded from the Web site of International Arctic Buoy Programme (IABP), Polar Science Center at the University of Washington in Seattle, WA. The NOAA NCEP-NCAR CDAS-1 Daily Intrinsic MSL pressure data are downloaded from the IRI/LDEO Climate Data Library at Columbia University, New York.

REFERENCES

[1] D. S. Early and D. G. Long, "Image reconstruction and enhanced resolution imaging from irregular samples," *IEEE Trans. Geosci. Remote Sensing*, vol. 39, pp. 291–302, Feb. 2001.

[2] A. K. Liu, Y. Zhao, and S. Y. Wu, "Arctic sea ice drift from wavelet analysis of NSCAT and special sensor microwave imager data," *J. Geophys. Res.*, vol. 104, pp. 11 529–11 538, 1999.

[3] A. K. Liu and D. J. Cavalieri, "Sea-ice drift from wavelet analysis of DMSP SSM/I data," *Int. J. Remote Sens.*, vol. 19, pp. 1415–1423, 1998.
[4] A. K. Liu, Y. Zhao, and W. T. Liu, "Sea-ice motion derived from satellite agrees with buoy observations," *EOS Trans. AGU*, vol. 79, pp. 353–359, 1998.
[5] Q. P. Remund and D. G. Long, "Sea ice extent mapping using Ku-band scatterometer data," *J. Geophys. Res.*, vol. 104, no. C5, pp. 11515–11527, 1999.
[6] P. K. Yoho and D. G. Long, "Validation of seawinds on QuikSCAT cell location," in *Proc. IGRSS*, Sydney, Australia, July 9–13, 2001, pp. 508–510.
[7] D. G. Long, M. R. Drinkwater, B. Holt, S. Saatchi, and C. Bertoia, "Global ice and land climate studies using scatterometer image data," *EOS Trans. AGU*, vol. 82, no. 43, p. 503, Oct. 23, 2001.
[8] R. Kwok, A. Schweiger, D. A. Rothrock, S. Pang, and C. Kottmeier, "Sea ice motion from satellite passive microware imagery assessed with ERS and buoy ice motions," *J. Geophys. Res.*, vol. 103, pp. 8191–8214, 1998.
[9] Y. Zhao, A. K. Liu, and C. A. Geiger, "Arctic sea ice motion from wavelet analysis of SSM/I data," *J. AMSS*, vol. 4, pp. 313–322, 1998.
[10] C. A. Geiger, Y. Zhao, A. K. Liu, and S. Hakkinen, "Large-scale comparison between buoy and SSM/I drift and deformation in the Eurasian Basin during winter 1992–1993," *J. Geophys. Res.*, vol. 105, pp. 3357–3368, 2000.

Yunhe Zhao received the B.S. degree in computational mathematics from Xiamen University, Xiamen, Fujian, China in 1984, and both the M.S. and Ph.D. degrees in mathematics from North Dakota State University, Fargo, ND, in 1993 and 1997, respectively.

He has been with Caelum Research Corporation, Rockville, MD since May 1997, first as a Mathematical Analyst and then as a Senior Analyst. His job is to work on-site at the Oceans and Ice Branch, NASA Goddard Space Flight Center, Greenbelt, MD, to provide technical and programming support to the research projects led by Dr. Antony K. Liu. His research interests include numerical solutions of boundary integral equations, wavelet analysis and its applications, satellite remote sensing of sea ice, satellite image processing, and computer science.

Antony K. Liu received the B.Sc. degree from National Chung-Hsing University, Taiwan, R.O.C., in 1970, specializing in applied mathematics. He received the Ph.D. degree in mechanics at The Johns Hopkins University, Baltimore, MD, in 1976.

Before he joined NASA Goddard Space Flight Center, Greenbelt, MD, in 1986, he worked at Dynamics Technology, Inc., Torrance, CA, as a Research Scientist, Group Manager, and later a Section Head of Ocean Technology. He was promoted to his current position, Senior Scientist, in 1992 at the Oceans and Ice Branch, Laboratory for Hydrospheric Processes at NASA Goddard Space Flight Center. He has been a Principal Investigator of the ERS-1/2 program for international polar oceans research of the European Space Agency, JERS-1 verification program of Japan, and RADARSAT application development and research opportunity program of Canada. Currently, he is also a Principal Investigator of QuikSCAT in the Ocean Wind Vector science team and AMSR/ADEOS-II science team for sea–ice motion study using wavelet transform. He is responsible for the overall technical effort and has lead responsibility for the development of satellite image processing algorithms, as well as wavelet analysis of AMSR and SeaWinds images for merged daily sea–ice motion and deformation maps in the Arctic. His research interests involve air–sea–ice interaction, satellite image processing, coastal monitoring, and nonlinear internal wave study.

David G. Long (S'80–SM'98) received the Ph.D. degree in electrical engineering from the University of Southern California, Los Angeles, in 1989.

From 1983 to 1990, he was with the Jet Propulsion Laboratory (JPL), Pasadena, CA, where he developed advanced radar remote-sensing systems. While at JPL, he was the Project Engineer on the NASA Scatterometer (NSCAT) Project, which was flown aboard the Japanese Advanced Earth Observing System (ADEOS) from 1996 to 1997. He also managed the SCANSCAT project, the predecessor to SeaWinds. He is currently a Professor in the Electrical and Computer Engineering Department, Brigham Young University, Provo, UT, where he teaches upper division and graduate courses in communications, microwave remote sensing, radar, and signal processing. He is the Principle Investigator on several NASA-sponsored interdisciplinary research projects in remote sensing, including innovative radar systems, spaceborne scatterometery of the ocean and land, and modeling of atmospheric dynamics. He is a member of the NSCAT and SeaWinds Science Working Teams. He has numerous publications in signal processing and radar scatterometery. His research interests include microwave remote sensing, radar theory, space-based sensing, estimation theory, computer graphics, signal processing, and mesoscale atmospheric dynamics.